8th International Symposium on Magnetic Bearing
August 26-28, 2002, Mito, Japan

SUPERCONDUCTING BEARINGS ASSISTED BY SELF-SENSING AMBS IN LIQUID NITROGEN

Mochimitsu Komori
Dept. of Mechanical System Engineering, Kyushu Institute of Technology
komori@mse.kyutech.ac.jp

Chiaki Shiraishi
Department of Mechanical System Engineering, Kyushu Institute of Technology
Chiaki@mse.kyutech.ac.jp

ABSTRACT

This paper describes newly developed superconducting magnetic bearings (SMBs) assisted by self-sensing active magnetic bearings (AMBs). The self-sensing AMBs detect the gaps between rotor and electromagnets. The principle of the self-sensing sensors is based on a differential transformer. The sensitivity in liquid nitrogen is almost equal to that in the air. The sensor is found to be useful in liquid nitrogen at 77 K (-196 °C). Moreover, the sensors are applied to the SMBs. Dynamics of the SMBs with self-sensing AMBs are discussed. From the results, it is found that the system is useful and promising.

INTRODUCTION

Applying high T_c superconductors to active magnetic bearings (AMBs) as a levitation mechanism is very promising [1]-[3]. Our group has been studying hybrid magnetic bearing (HMBs) composed of superconducting magnetic bearings (SMBs) and active magnetic bearings (AMBs) [3]. If the HMBs are used in liquid nitrogen, they don't work well. It is because displacement sensors for the HMBs don't work due to the low temperature in liquid nitrogen. In order to use displacement sensors working in liquid nitrogen, very expensive sensors which are especially developed have to be bought.

Thus, we have newly developed a self-sensing displacement sensor for the SMBs used at an extremely low temperature in liquid nitrogen. In this paper, the displacement sensors are evaluated but in liquid nitrogen also in the air. Dynamics of the SMBs with self-sensing AMBs are also discussed. This type of displacement sensor available at low temperatures has rarely been reported elsewhere.

SYSTEM

Total System

The experimental setup for the superconducting magnetic bearings (SMBs) assisted by self-sensing active magnetic bearings (AMBs) was built as shown in Figure 1. The system consists of a rotor (shaft), a pair of SMBs with doughnut-shaped superconductors ($Y_1Ba_2Cu_3O_X$, ϕ45 mm $\times$16 mm), a pair of AMBs with four electromagnets, and a driving motor. The rotor consists of a set of four ring magnets for the SMB and a pair of iron parts for the AMB, and measures 24 mm in diameter, 160 mm in length and 0.37 kg in weight. The details of the structure are almost the same as those in Reference [3]. The right and left ends of the rotor are supported by both the SMB and the AMB. Zero-bias technique is applied to the self-sensing AMBs for energy saving. That is, in the system the SMBs are more dominant than the AMBs, because the AMBs assist the SMBs.

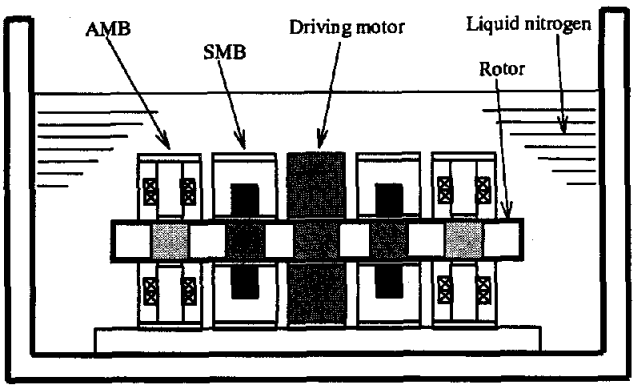

FIGURE 1: Experimental setup for the SMBs assisted by self-sensing AMBs.

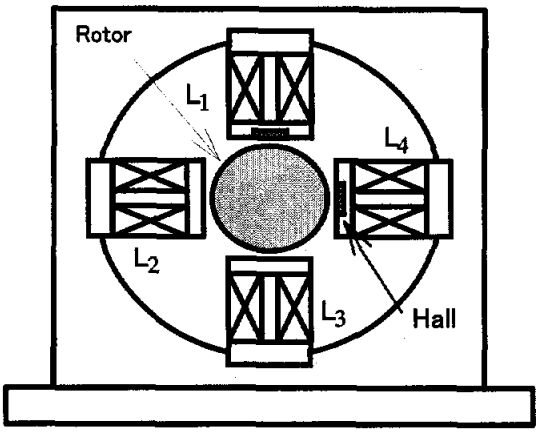

FIGURE 2: Schematic illustration of the motor.

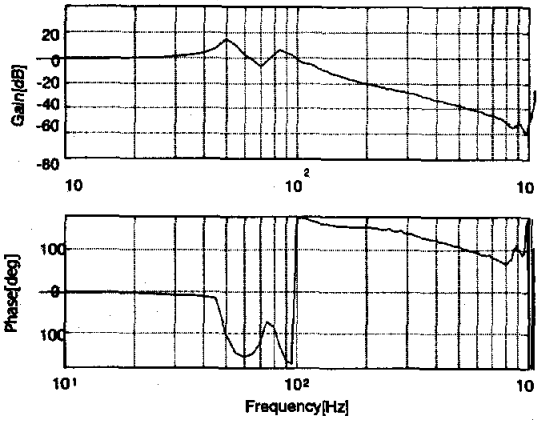

FIGURE 3: Compliance of the left SMB.

Figure 2 shows a schematic illustration of the side view of the motor which works in liquid nitrogen. The motor consists of a rotor with permanent magnet (PM) and four electromagnets for driving it. Hall sensors are installed in the motor to detect the rotation angle of the motor. Since the Hall sensors detects the rotation angle, the rotor spins without any contacts to the electromagnets. In this paper, the driving characteristics such as torque and displacement are discussed later.

Dynamic Model

In order to make the SMBs model, we measured the compliance of the SMBs supporting the rotor. In the experiment, the AMBs were used to vibrate the rotor supported by the SMBs. Figure 3 shows the compliance of the left SMB. We applied a 2nd order model to the experimental result, which is given by

$$m\ddot{x}_G + c\dot{x}_G + kx_G = f_{xL} + f_{xR} + f_{xd} \quad , \tag{1}$$

$$J\ddot{\theta} + c_r\dot{\theta} + k_r\theta = -\ell_b f_{xL} + \ell_b f_{xR} + m_{\theta d} \quad , \tag{2}$$

$$m\ddot{y}_G + c\dot{y}_G + ky_G = f_{yL} + f_{yR} + f_{yd} \quad , \tag{3}$$

$$J\ddot{\phi} + c_r\dot{\phi} + k_r\phi = \ell_b f_{yL} - \ell_b f_{yR} + m_{\phi d} \quad , \tag{4}$$

where x_G and y_G are displacements of the rotor, f_{ij} $(i=x,y,\ j=L,R)$ are attractive forces to the rotor, f_{id} $(i=x,y)$ are disturbances for the rotor, θ and ϕ are rotation angles of the rotor, m_{id} $(l=\theta,\phi)$ are moments of the rotor.

From Figure 3, we got various parameters as shown in Table 1. In the table, the parameters for the left SMB are shown like c/2 and k/2. Since γ is very small, the damping of the SMBs is found to be very small. This should be improved by using the AMBs. Using these parameters, theoretical compliance is produced. It is found that the theoretical compliance is almost equal to the measured compliance below 200 Hz. This shows that dynamic models for the SMBs are represented by 2nd order functions.

Self-sensing AMB

Figure 4 shows a block diagram for the self-sensing AMB. The system consists of a rotor, four electromagnets, some amplifiers, and displacement circuit. The outputs from the displacement circuits are applied to the computer. The principle of the self-sensing sensors is based on a differential transformer [4].

To simplify the explanation, the AMB has the upper

TABLE 1: Various parameters for the left SMB obtained by using the compliance

Cylindrical	
c/2 [N·s/m]	20.0
k/2 [N/m]	4.70×10^4
γ [-]	0.104
ω_n [rad/s]	5.34×10^2
ω_d [rad/s]	5.31×10^2
Conical	
$c_r/2$ [N·m·s]	7.98×10^{-3}
$k_r/2$ [N·m]	39.0
γ_r [-]	3.21×10^{-2}
ω_{nr} [rad/s]	3.14×10^2
ω_{dr} [rad/s]	3.14×10^2

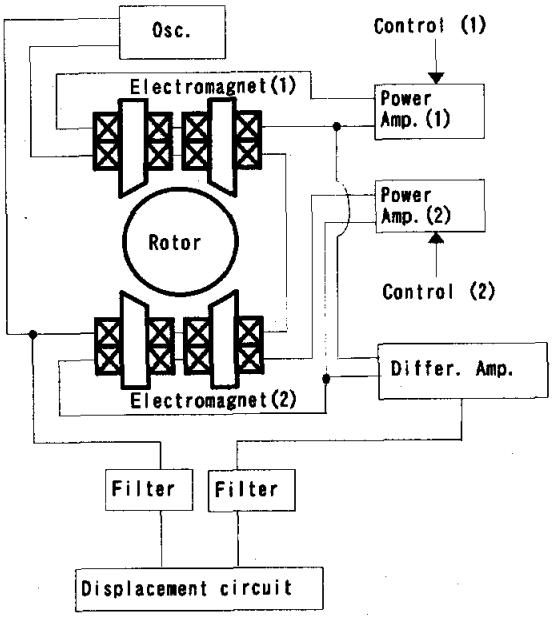

FIGURE 4: Block diagram for the self-sensing AMB.

and lower electromagnets with four coils. Two primary coils of the upper electromagnet are excited by the PWM amplifiers. The induced voltage is led to the secondary two coils for sensing the displacement. The induced voltage e_{x1} of the upper secondary coils is given by

$$e_{x1} = -M_{x1}\frac{dI_1}{dt}, \tag{5}$$

where M_{x1} and I_1 are mutual inductance and control current to the upper primary coils, respectively. Assuming that there is no leakage flux, mutual inductance M_{x1} becomes

$$M_{x1} = \frac{\mu_0 N^2 S}{x_0 + x}, \tag{6}$$

where x_0, x, N, S, and μ_0 are average air gap, rotor displacement, number of coil turns, cross-sectional area of electromagnet, and permeability of vacuum, respectively. Substituting Equation (6) to Equation (5), the induced voltage of the upper secondary coils is given by

$$e_{x1} = -\frac{\mu_0 N^2 S}{x_0 + x}\cdot\frac{dI_1}{dt}. \tag{7}$$

In the same manner, the induced voltage of the lower secondary coil is given by

$$e_{x2} = \frac{\mu_0 N^2 S}{x_0 - x}\cdot\frac{dI_2}{dt}, \tag{8}$$

where I_2 is control current to the lower primary coils. Equations (3) and (4) show that the induced voltages e_{x1} and e_{x2} are inversely proportional to the rotor displacement x. Assuming $I_1 = I_2 = I$ and $x_0 >> x$, the differential output voltage e between the upper and lower induced voltages is given by

$$e \cong \frac{2\mu_0 N^2 S x}{x_0^{\,2}}\frac{dI}{dt}. \tag{9}$$

The differential output voltage e is proportional to the rotor displacement x. This shows that the rotor displacement is detected by this method. A zero-bias current is applied to the electromagnet using the upper and lower secondary coils.

Figure 5 shows relationships between output voltage and rotor displacement at room temperature in (a) the vertical direction and (b) the horizontal direction. Both

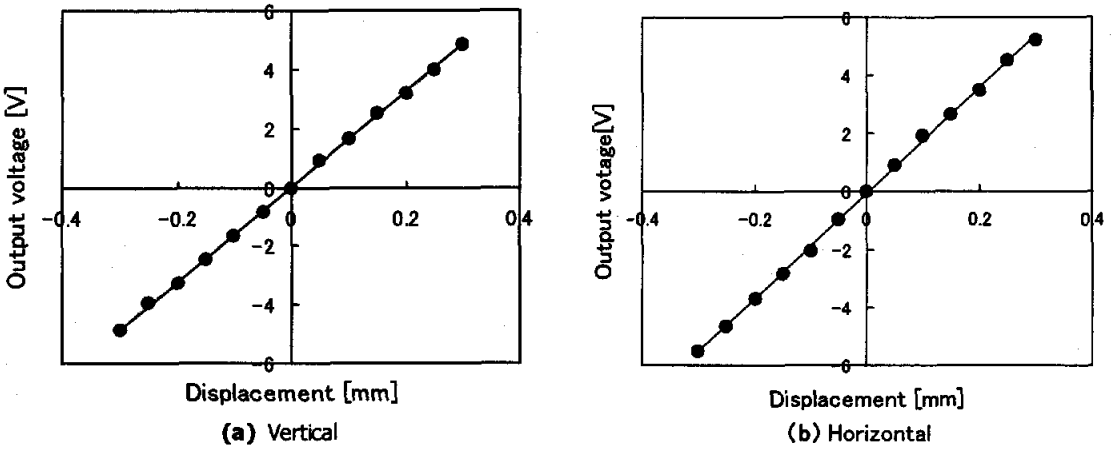

FIGURE 5: Relationships between output voltage and rotor displacement at room temperature in (a) the vertical direction and (b) the horizontal direction.

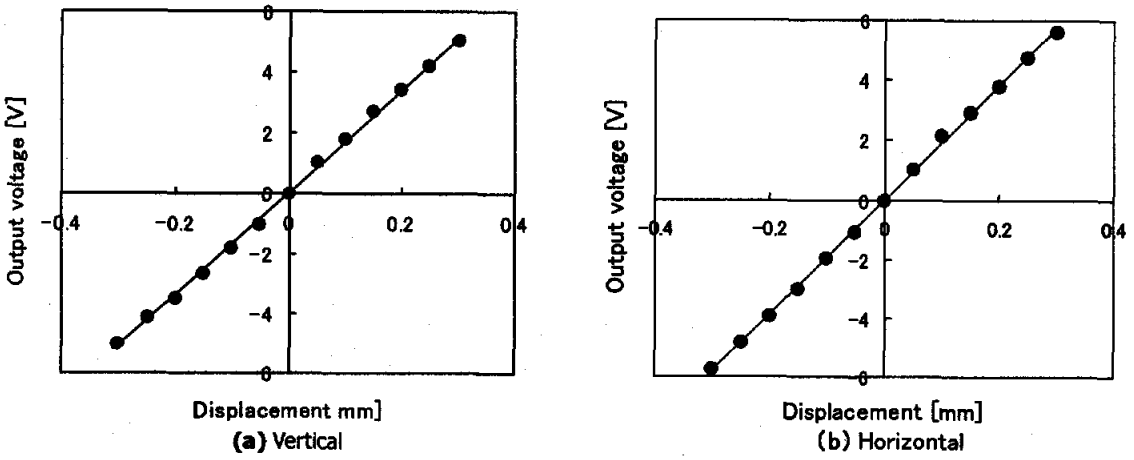

FIGURE 6: Relationships between output voltage and rotor displacement at liquid nitrogen temperature in (a) the vertical direction and (b) the horizontal direction.

relationships in Figures 5(a) and (b) are almost linear and show gains of ≅ 16.1 V/mm and ≅ 18.2 V/mm in the displacement range from -0.3 to 0.3mm. Figure 6 shows relationships between output voltage and rotor displacement at liquid nitrogen temperature in (a) the vertical direction and (b) the horizontal direction. The relationships in Figures 6 (a) and (b) are almost linear in the displacement range from -0.3 to 0.3 mm. The gains of Figure 6(a) and (b) are ≅ 17.1 V/mm and ≅ 19.2 V/mm, respectively. It is very surprising that the results in Figure 6 are in good agreement with the results in Figure 5 in spite of its extremely low temperature environment. This is because magnetic properties of the electromagnet don't change essentially in liquid nitrogen and because the output doesn't depend on the temperature so much.

Control

Zero-bias currents are applied to the AMBs in order to reduce energy loss. The applied voltages to the amplifiers are represented by

$$V_{ij1} = -\frac{1}{k_a}\sqrt{\frac{f_{ij1}}{k}}\left(\ell_a - w_i\right), \tag{10}$$

$$V_{ij2} = -\frac{1}{k_a}\sqrt{\frac{|f_{ij2}|}{k}}\left(\ell_a + w_i\right), \tag{11}$$

where $i = x, y$ and $j = L, R$. Equations (10) and (11) can be written as

$$V_{ij} = sign\left(f_{ij}\right)\frac{1}{k_a\sqrt{k}}\sqrt{|f_{ij}|}\left\{\ell_a - sign\left(f_{ij}\right)w_i\right\}, \tag{12}$$

where

$$sign\left(f_{ij}\right) = \begin{cases} 1, & f_{ij} > 0 \\ 0, & f_{ij} = 0 \\ -1, & f_{ij} < 0 \end{cases} \tag{13}$$

and the force in the x direction is considered to be positive in Equation (12). Furthermore, Equation (12) can be written as

$$V_{ij1} = \begin{cases} -V_{ij} & \left(V_{ij} \geq 0\right) \\ 0 & \left(V_{ij} < 0\right) \end{cases} \tag{14}$$

$$V_{ij2} = \begin{cases} 0 & \left(V_{ij} \geq 0\right) \\ V_{ij} & \left(V_{ij} < 0\right) \end{cases} \tag{15}$$

Equations (14)-(15) indicate that the current is applied to one of the electromagnets facing each other. Therefore, the rotor position is controlled by using the voltages to the electromagnets according to Equations (10) - (15). The details about this method have already been reported in Reference [5].

In the experiments, the rotor mass is supported by the SMBs assisted by the AMBs. And the AMBs are performed by using the zero-bias control technique above mentioned. The controller gains were tuned by using the stability analysis for open loop system. Because the purpose of the controller is the suppression of the vibrations near the resonance frequency, the closed loop gain is made flat in the lower frequency range.

EXPERIMENTS AND RESULTS

The dynamics of the SMBs supported by the self-sensing AMBs are studied. First, impulse responses for the SMBs without AMBs and the SMBs with AMBs were investigated. Impulse forces were applied to the left side of the rotor in the vertical and horizontal directions using

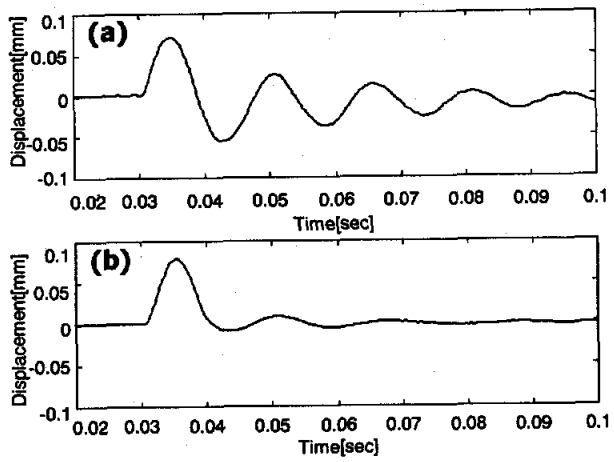

FIGURE 7: Impulse responses of (a) the SMBs and (b) the SMBs with AMBs in the vertical direction.

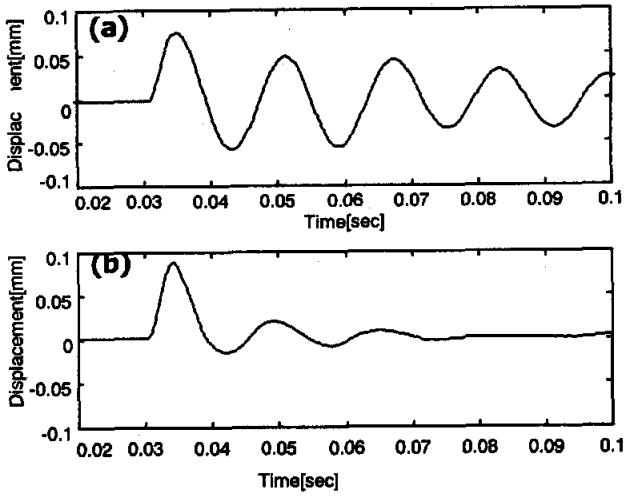

FIGURE 8: Impulse responses of (a) the SMBs and (b) the SMBs with AMBs in the horizontal direction.

a small hammer. During the experiments, the systems were immersed in liquid nitrogen. The maximum displacement is smaller than 0.1 mm.

Figure 7 shows the Impulse responses of (a) the SMBs without AMBs and (b) the SMBs with AMBs in the vertical direction. The experiments were performed in liquid nitrogen. As shown in Figure 7, damped free vibration curves are observed in both impulse responses. The vibration curves seem to decrease exponentially. The damping of vibration curve in Figure 7(b) is larger than that in Figure 7(a). This is because the SMBs assisted by self-sensing AMBs work well. However, the damping isn't so effective in Figure 7(b) in comparison

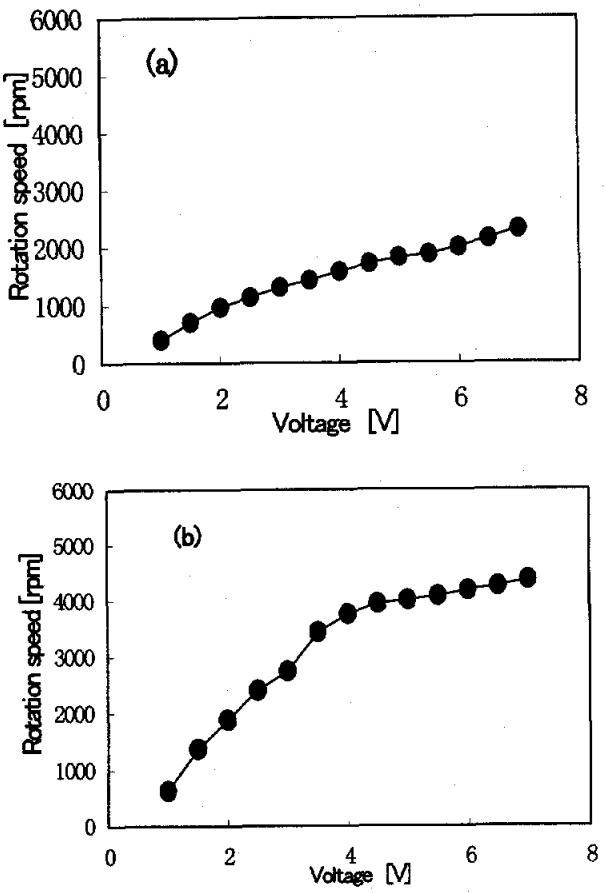

FIGURE 9: Relationships between rotation speed and applied voltage to the driving circuit of the motor in (a) liquid nitrogen and (b) the air.

with other AMB systems, because the non-bias method is adopted for the self-sensing AMBs.

Impulse responses for the SMBs without AMBs and the SMBs with AMBs in the horizontal direction were measured. Figure 8 shows the impulse responses of (a) the SMBs without AMBs and (b) the SMBs with AMBs in the horizontal direction. As shown in Figure 8, the impulse responses are the same as those in Figure 7. It is found that the settling time of the SMB in Figure 8(b) is smaller than the time in Figure 8(a). Anyway, the self-sensing displacement sensors are found to be applicable to our SMBs working in liquid nitrogen.

Figure 9 shows the relationships between rotation speed and applied voltage to the driving circuit of the motor in (a) liquid nitrogen and (b) the air. The applied voltage is equal to the voltage given to the electromagnets. Thus, with increasing applied voltage, the rotation speed increases in both liquid nitrogen and the air. The rotation speeds in Figure 9(b) are almost twice as large as those in Figure 9(a). This is because the viscosity of liquid nitrogen is stronger than the air

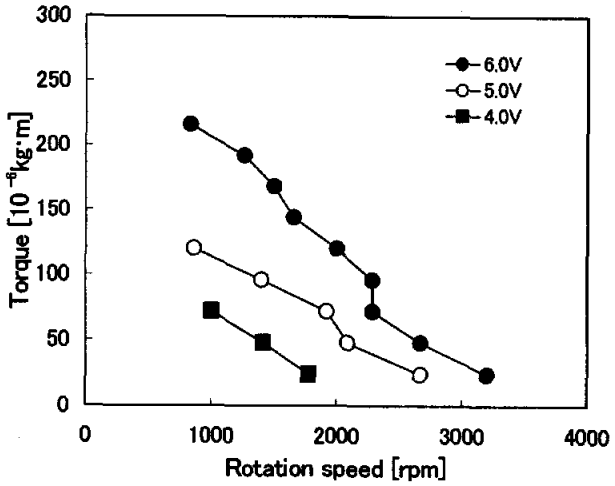

FIGURE 10: Relationship between motor torque and rotation speed for various applied voltages to the motor in the air

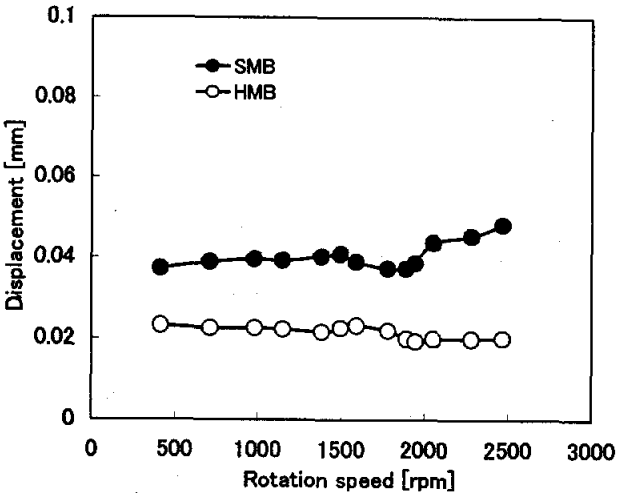

FIGURE 11: Relationships between displacement and rotation speed in the vertical direction.

viscosity and because the resistance of coils in liquid nitrogen is smaller than that in the air. The coil inductance seems to limit the rotation speed.

Figure 10 shows the relationship between motor torque and rotation speed for various applied voltages to the motor in the air. With increasing rotation speed, each torque decreases. As the applied voltage increases, the torque becomes large. Though the experiments were performed in the air, the torque in liquid nitrogen is equal to that in the air in case of the same speed.

Finally, we evaluated the rotor displacement during the rotation. Figure 11 shows the relationship between displacement and rotation speed in the vertical direction. The black circles and white circles indicate the results for the SMBs without AMBs and the SMBs with AMBs. The experiment was performed in liquid nitrogen. In Figure 11, the displacement for the SMBs without AMBs is about 0.04 mm in the speed range lower than 2500 rpm. The displacement for the SMBs assisted by self-sensing AMBs is about 0.02 mm. The displacement for the SMBs without AMBs is twice as large as that for the SMBs with AMBs. This is because the SMBs assisted by the AMBs suppress the vibrations more than the SMBs. From these results above mentioned, the SMBs assisted by self-sensing AMBs are useful for suppressing the rotor vibrations.

CONCLUSIONS

We have developed the SMBs assisted by self-sensing AMBs working at extremely low temperature. The experimental results show that the displacement sensors has a linear relationship between differential output voltage and rotor displacement. The result of self-sensing at room temperature is in good agreement with the result at liquid nitrogen temperature. From the results of impulse responses, the damping of vibration curve for the SMBs with AMBs is more effective than that for the SMBs without AMBs. It is found that the SMBs assisted by the AMBs suppress the vibrations more than the SMBs. From these results above mentioned, the SMBs assisted by self-sensing AMBs are useful for suppressing the rotor vibrations even in the extremely low temperature environment.

REFERENCES

1. F. C. Moon and P.-Z. Chang, High-speed rotation of magnets on high T_c superconducting bearings, Appl. Phys. Lett., vol. 56, 1990.
2. H. J. Borneman and M. Sander, Conceptual system design of a 5 MWh/100 MW superconducting flywheel energy storage plant for power utility applications, IEEE Trans. Appl. Superconduct., vol. 7, 1997.
3. M. Komori, S. Matsuoka, and S. Fukata, Evaluation of a hybrid-type superconducting magnetic bearing system, IEEE Trans. Appl. Superconduct, vol. 6, 1996.
4. K. Matsuda and Y. Okada, Self-sensing magnetic bearing using the principle of differential transfomer, 5th Int. Symp. on Magnetic Bearings, Kanazawa, Japan, Aug., 1996.
5. M. Komori, M. Kumamoto and H. Kobayashi, A hybrid-type superconducting magnetic bearing system with nonlinear control, IEEE Trans. on Appl. Superconduct., vol.8, 1998.